Malaysian Journal of Science 21A: 65-70 (2002)

Pulsed plasma x-ray and EUV sources

C.S. Wong

Plasma Research Laboratory, Physics Department, University of Malaya, 50603 Kuala Lumpur, Malaysia.

ABSTRACT Recently, the development of pulsed plasma devices as X-ray and EUV sources for applications in nanolithography and microscopy has been the research topic in many laboratories around the world. In this paper, we review the research effort on three types of pulsed plasma sources being carried out in this laboratory. The devices reviewed are the plasma focus and the vacuum spark as X-ray sources; and the pulsed capillary discharge as EUV source.

(Pulsed plasma, EUV, X-ray, Nanolithography, Microscopy)

INTRODUCTION

It is clear that the development of short wavelength (EUV to X-ray) sources for nanolithography is critical for the next generation of microchip fabrication where nano-scale patterns are to be replicated [1]. Three main categories of sources are being considered currently for applications in X-ray or EUV lithography. These are: (1) the conventional electron beam-target stems; (2) the synchrotron; and (3) the pulsed plasma systems. Of these, the first category of devices are mainly useful in the harder region of the X-ray spectrum so their application potential in lithography is limited since the presently available resists are sensitive only in the longer than 1 nm spectral region. The synchrotron source has already been successfully demonstrated in t he production o f working integrated circuits [1] and also in contact microscopy of biological specimen [2]. However, due to the scale of the facility they may not be suitable for actual industrial production operation. On the other hand, the pulsed plasma sources, although still in the development stage, offer several advantages over the other two categories of X-ray and EUV sources. These include compactness, low cost, simple operation and high radiation flux. Recently, with the successful demonstration of amplification of short wavelength radiation in the pulsed capillary discharge [3], the use of plasma pumped x-ray laser source may soon be available for effective implementation of X-ray and EUV lithography and microscopy for industrial applications.

Plasmas can be heated to x-ray emitting temperatures (> 10^6 K) either by pulsed electrical discharge or by high power pulsed lasers. Examples of pulsed plasmas heated by electrical discharge are the Z-pinches [4], the plasma focus [5], the vacuum spark [6] and the capillary discharge [3]. The laser produced plasma is the most extensively studied plasma x-ray source in the past. However, due to the two stages of energy conversion from electrical to optical and then from optical to x-ray, the overall efficiency of this type of plasma x-ray source is relatively low. In view of this, the electrical discharge produced plasmas such as the plasma focus and the vacuum spark are being considered more favorably recently. On the other hand, the capillary discharge is a good source of radiation in the EUV region and it is being investigated both as an intense high repetition rate point source as well as a pump source for soft X-ray/EUV laser.

In the Plasma Research Laboratory at University of Malaya, three types of pulsed plasma x-ray sources are currently being study. These are the plasma focus, the vacuum spark and the capillary discharge. Some of the results obtained will be discussed in this paper.

THE PLASMA FOCUS

The plasma focus device being studied is of the Mather type powered by a single 15 kV, 30 μF capacitor. It was originally designed for optimum operation in deuterium for nuclear fusion study [7]. When argon is used as the filling gas, copious x-ray emission is detected. The dynamics of the plasma focus discharge may be divided into three phases: the lift-off phase, the axial run-down phase and the radial compression phase. The final hot dense plasma is produced at the end of the radial compression phase. The x-ray emission from this plasma focus device with argon and argon-hydrogen admixture as the filling gas has been studied by using various diagnostics including time-resolved PIN diodes, scintillator- photomultiplier detector [8]; time-integrated and time-resolved pinhole imaging [9-10] and time-resolved multichannel diode x-ray spectrometer [11]. These measurements show that the plasma produced by the plasma focus device consists of a plasma column of about 1 to 2 mm diameter and 10 to 50 cm length, with spots of distinctly high x-ray intensity embedded in it. An example [12] of the time-resolved x-ray pulse measured from a typical shot of the argon plasma focus discharge is shown in Fig. 1(a). The corresponding time-integrated pinhole image of the x-ray source structure is shown in Fig. 1(b).

Spectral analysed of the x-ray emission from the focused plasma show that its spectrum is initially dominated by the free-free and free-bound emission originated from the hot dense focused plasma. This corresponds to pulse 1 in the signal shown in Figure 1(a). The estimated electron temperature is about 2 keV and the peak of the x-ray emission spectrum is expected to be at a wavelength of around 3 Å. The subsequent two pulses are broader and they are found to be heavily contaminated with copper K_α line radiation indicating an increase in copper impurity in the argon plasma. The copper impurity may be introduced into the system by the bombardment of the copper anode by electron beam.

THE VACUUM SPARK

The vacuum spark is a simple pulsed plasma device, which is capable of producing intense bursts of soft and hard x-rays. Conventionally, the discharge of a vacuum spark is initiated either by an auxiliary sliding spark at the cathode surface [14], or by focusing a powerful pulsed laser beam onto the tip of the anode [9]. In the case of the sliding spark triggering, the sliding spark acts as a source of electrons, which are attracted towards the anode by the electric field, bombarding it to produce a puff of weakly ionized plasma of the anode material. Subsequent passage of current through this weakly ionized plasma produces plasma of high density and temperature. In the case of the laser triggering, the weakly ionized pre-breakdown plasma is produced by the laser-target interaction. The eventual plasmas formed after breakdown of the main discharge are found to be identical in the two cases. Recently, a new method of triggering the vacuum spark has been proposed and tested successfully in this laboratory [15]. In this method, a hollow cathode configuration has been incorporated into the vacuum spark system so as to utilise the transient hollow cathode effect to generate an intense on-axis electron beam, which will bombard at the anode tip to initiate the main discharge. With this new method of triggering, the vacuum spark system has been optimized to produce the hot dense plasma spots as shown in Figure 2 consistently [16].

The vacuum spark triggered by the transient hollow cathode discharge electron beam which is being studied in t his laboratory (UMVS-III) is powered by a single 20 kV, 1.85 μF. The electron temperature of the plasma produced is measured to be about 2 to 3 keV, with a density in the range of 10^{20} to 10^{21} cm^{-3}. Hot dense plasma spot emitting intense x-ray is observed consistently. The size of this hot spot is measured [16] to be of the order of 100 to 200 μm. The x-ray emission spectrum of the vacuum spark plasma is found to consist of predominantly the continuum radiation. Due to the high particle density, the X-ray emission is intense enough to allow single shot measurement of the spectrum by using a solid state based X-ray spectrometer (eg. AMPTEK XR-100CR) as shown in Figure 3. However, at an electron temperature o f 2 t o 3 k eV only, t he hydrogen-like CU^{28+} ionic specie may not be prominent and hence the Cu Kα line cannot be observed in a single shot exposure.

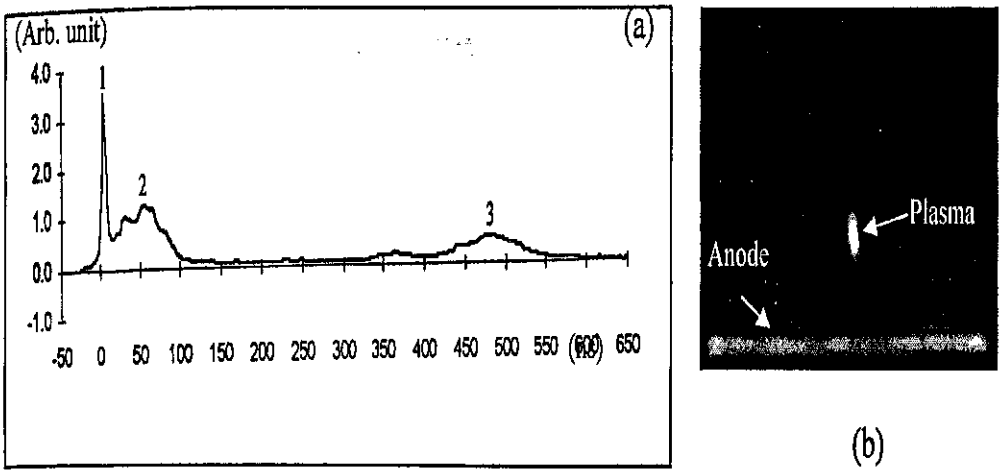

Figure 1. (a) Time-resolved PIN diode (with 24 μm Aluminised mylar) x-ray signal of an argon plasma focus discharge.
(b) X-ray pinhole image of the focussed plasma.

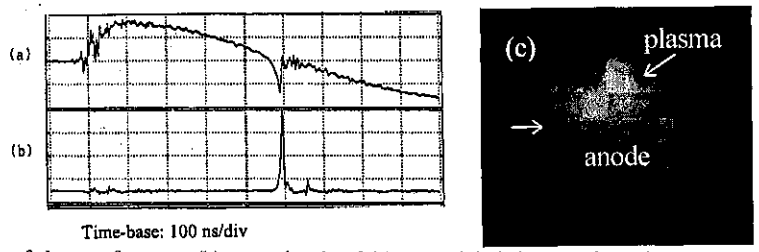

Figure 2. (a) Rate of change of current, (b) x-ray signal and (c) x-ray pinhole image o f a typical vacuum spark discharge.

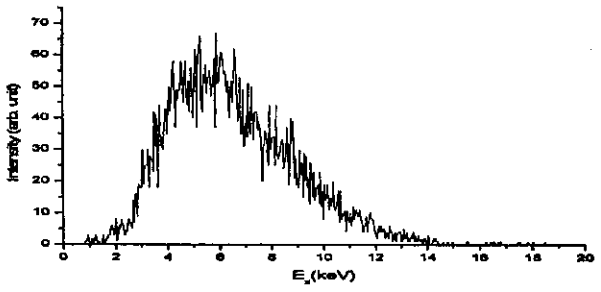

Figure 3. Typical X-ray emission spectrum obtained with single exposure from a copper anode UMVS-III vacuum spark plasma at $T_e = 2.8$ keV.

The vacuum spark has also been operated with ower input electrical energy of 20 kV, (3 - 22) F. With such a low input energy, the plasma vill not be heated to high enough temperature to mit in the X-ray region. This regime of peration of the vacuum spark is referred to as he flash X-ray tube [17]. In this case X-ray is roduced by the interaction of the transient hollow cathode electron beam and the anode tip which acts as the thick target. The spectrum of the X -ray produced consists of predominantly the K_α line radiation of the anode material. This X-ray source, although has low intensity, may still be useful as a point source for microscopy of small biological sample.

PULSED CAPILLARY DISCHARGE

The pulsed capillary discharge has been shown to be a copius source of EUV and soft x- ray [18]. Recently, due to the successful demonstration of amplification of the 3s $^1p_1$ -3p $^1S_0$ line of Ne-like Ar at λ = 46.9 nm in a capillary discharge [3], this device has attracted much research interests from various researchers [19-21].

In this laboratory, work on the pulsed capillary discharge started since 1993. Our main interest is to develop the pulsed capillary discharge as a high repetition rate EUV source for nanolithography. Various configurations have been tested to achieve a high brightness, reproducible high repetition rate emission. One of these configurations is the UMCD-VI which consists of a 2 mm diameter, 100 mm long quartz capillary as shown in Figure 4.

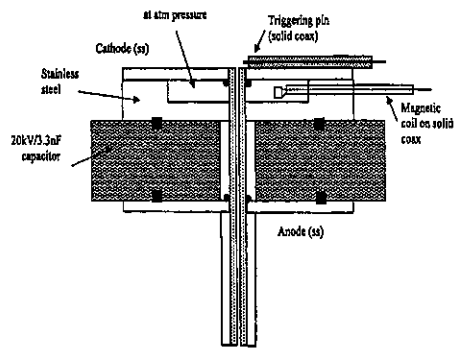

Figure 4. Schematic layout of UMCD-VI pulsed capillary discharge.

The discharge is powered by six door knob ceramic capacitors each rated at 20 kV, 3.3 nF. The discharge is triggered by the on-axis electron beam produced by the transient hollow cathode effect [6] which has been integrated into the present capillary discharge system. This system has been able to produce near critically damped discharge as shown in Figure 5. This indicates that the plasma is being heated resistively. The plasma emission recorded by an unfiltered XRD shows that its intensity rises almost in phase with the current.

It is clear that due to the low input electrical energy (4 J), and the relatively slow discharge (<2 x 10^{11} A/s), the plasma has not been heated up to a sufficiently high state of ionization. Work is now being carried out to reduce the inductance in order to achieve a faster risetime for the discharge current as well as to upgrade the input electrical energy.

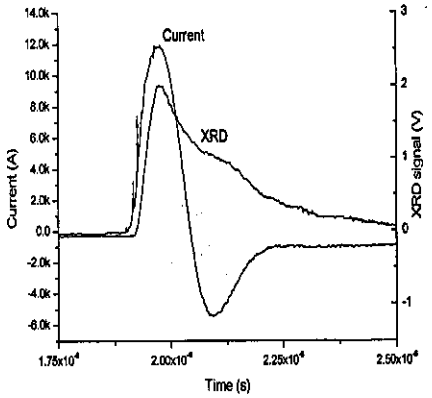

Figure 5. The discharge current and EUV emission signals of UMCD-VI

CONCLUSION

We have briefly described three types of plasma devices, which have great potential to be developed into pulsed X-ray and/or EUV sources. Much work is needed to further characterise their X-ray and EUV emission and to optimize their performance. The goal is to produce a high brightness source, either in the point source or laser configuration, suitable for industrial scale nanolithography process.

Acknowledgement The work reviewed in this paper is part of the results of the research effort of the Plasma Research Group at the Physics Department, University of Malaya since the 1970's. Under RMK7, research on the plasma focus, vacuum spark and the pulsed capillary discharge was partially supported by IRP A project 09-02-03-0364.

REFERENCES

1. Ohki, Shigehisa and Ishihara, Sunao, *Microelectronic Engineering* **30**, 171 (1996).
2. Kirz, J. and Sayre, D. *Soft x-ray microscopy of biological specimen* in "Synchrotron radiation research", eds. Doniach, S. and Winick, H., Plenunl Press, N.Y. (1980)
3. Rocca, J.J. et. al., *Phys. Rev. Lett.* **73**, 2192(1994).
4. Bailey, J. et al, *Appl. Phys. Lett.*, **40,** 33 (1982).

5. Kato, Y. and Be, S.H., *Appl. Phys. Lett.* **48**, 686 (1986).
6. Wong, C.S. and Lee, S., *Rev. Sci. Instrum.* **55**, 1125 (1984).
7. Lee, S. et al, *Am. J. Phys.* **56**, 62 (1988).
8. Moo, S. and Wong, C.S., *Laser and Particle Beams* **13**, 129 (1995)
9. Wong, C.S. et al, *Rev. Sci. Instrum.* **59**, 391 (1988).
10. Wong, C.S. et al, *Mal. J. Sci.* **17**, No.2 (in press).
11. Wong, CS et al, Five Channel Diode X-ray Spectrometer -Instruction Manual, ICAC-UM/DXS
12. Ng, CM" MSc thesis, University of Malaya (1996)
13. Wong CS et al, p626, Proc 5th Asia Pacific Physics Coni, World Scientific, Singapore (1994)
14. Lee, S and Conrads, *H" Phys Lett 57A*, 233 (1976)
15. Wong, CS et al, *IEEE Trans Plasma Sci* **23**, 265 (1995)
16. Gopal, NJ" MSc Thesis, University of Malaya (1995)
17. Bradley, DA" Wong, CS and Ng, *KH" Appl Radiation & Isotopes* **53**, 691 (2000)
18. McCorkle, *RA" Appl Phys A* **26**, 261(1981)
19. Choi, P et al, BEAMS 96
20. Shin, HJ" Kim, DE and Lee, *TN" Phys Rev E* **50**, 1376 (1994)
21. Steden, C and KUttZe, *HcJ" Phys Lett A* **151**, 534 (1990)

Malaysian Journal of Science **21A**: 71-76 (2002)

Experimental set up for low-angle x-ray scattering system used for the characterization of materials

N. A. Hussein [1,3], A. Shukri [1] and A. A. Tajuddin [1,2]

[1] *School of Physics, Universiti Sains Malaysia, 11800 Penang, Malaysia.*
[2] *Abdus Salam International Center for Theoretical Physics, Strada Costiera, 11-34014 Trieste, Italy*
[3] *Permanent address: Department of Physics, Faculty of Science, Garyounis University, Benghazi, Libya.*

ABSTRACT Elastic X-ray scattering at low angles will give rise to diffraction patterns of unique signatures that can be exploited in the identification of various materials. The design criteria for setting up a low angle X-ray scattering system (LAXS) and its parameters of influence will be discussed individually. The LAXS system under construction at the School of Physics, USM, will be introduced.

(LAXS, EDXRD, Elastic X-ray scattering, Characterization of materials)

INTRODUCTION

Characterization and identification of materials have been achieved by many methods, destructive or nondestructive, employing ionizing or non-ionizing radiation and applied in the industrial, medical or other fields. Whatever, the method used on any material of interest which belongs to any of these various fields; the end result is obtaining some information that will relate to the substance under scrutiny.

The X-ray diffraction technique was, and is still being employed, as a method for characterization of crystalline materials; the familiar subject of crystallography. X-ray diffraction by large molecules, which show non-crystallinity with some order on the local scale, has also been done. Since the spacing of such molecules is quite large, in the order of tens and hundreds of interatomic spacing, the restriction to the use of small scattering angles is clearly observed [1].

X-ray radiation has been used in imaging for many years in the field of radiology, which is a well-established science. X-ray scattering in this field is considered a problem [2] that reduces contrast and signal to noise ratio of the image. Such problematic scattering must be overcome and various procedures have been used by many authors [3,4], in order to minimize the effect of this scattering on the quality of imaging.

Due to the dominance of scattering cross-sections over absorption cross-sections for common materials and in the energy range of interest [5-7], scattering can be a useful tool in the characterization of materials.

THEORY

Coherent scattering has been dismissed as a process for identification of materials because of its small contribution to the attenuation coefficient compared with incoherent scattering. Coherent scattered radiation does not depend on energy and its angular dependence is forward peaking, i.e. the differential scattering probability is peaked at zero and therefore indistinguishable from transmitted radiation, and in such case it is a reducing quality process [8].

However, calculations by Johns and Yaffe [9] using single scatter showed that in the diagnostic energy range, the differential scattering cross-section for coherent scattering did not peak at zero angle as was previously believed but at an angle larger than zero. In fact the differential coherent scattering cross-section at zero almost vanishes. The work of the above authors on water, an amorphous material, concluded that the maximum scattering probability occurred at an angle 3.8° for 60 keV photons. They attributed this to intermolecular interference. Their work also showed that coherent scattering was much greater than incoherent scattering at low angles,

and it contributes significantly to the total scattering process.

Scattering can be from a single free electron, the classical case of oscillating charge that emits radiation of the same frequency as photon impinging on it. This is known as the "Thomson scattering" and in this case the differential scattering cross-section for unpolarized X-ray is given by

$$\frac{d\sigma}{d\Omega} = \frac{1}{2} r_o^2 (1+\cos^2\theta) \qquad (1)$$

where, r_o is the classical electron radius sometimes known as the *Thomson scattering length* with a value of $2.82\times10^{-15}m$ whilst θ is the scattering angle. Scattering can also be from bound electrons in an atom of atomic number Z and in this case, Thomson scattering from individual electrons in the atom is coherent. Therefore, in the forward direction the amplitudes of the scattered waves have to be added before squaring to give intensity (or cross-section). Also, the scattered waves undergo destructive interference in all other directions.

The above outline leads to the differential atomic coherent scattering cross-section that is given by

$$\frac{d\sigma}{d\Omega} = \frac{1}{2} r_o^2 (1+\cos^2\theta) F^2(Z,q) \qquad (2)$$

where, $F(Z,q)$ is known as the atomic scattering factor or form factor. This factor is a function of Z and momentum transfer, q which, relates to scattering angle and wavelength of radiation, and its role is to include the coherent scattering from all parts of the atom. This scattering is known as "Rayleigh scattering".

Interference can be attributed to be due to three basic routes: first between scattered waves of electrons in the same atom of object molecule, secondly between scattered waves of electrons of neighbouring atoms within the same object molecule, and thirdly between scattered waves of different molecules (intermolecular).

X-ray scattering at low angles is a coherent or elastic process due to the high probability of its cross-section over incoherent (inelastic) Compton scattering cross-section at low angles. Furthermore, if the object material has some regular order, be it short or long order, then interference can occur between coherent scattered X-rays photons from adjacent atomic planes, at some low angle θ. Diffraction will then occur and is governed by the Bragg law given by

$$n\lambda = d \sin\frac{\theta}{2} \qquad (3)$$

where n is the order of diffraction, λ is the wavelength of incident X-ray photon, θ is the scattering angle, and d is the interatomic spacing. The diffraction pattern will be a characteristic of that object material.

Inspection of Equation (3) shows clearly two distinctive methods of obtaining diffraction patterns. Keeping incident wavelength λ of X-ray photon fixed (using a monoenergetic photon) and sweeping the various angles θ to obtain the diffraction pattern. This is known as the angular dispersive method and it is common in the field of crystallography. The alternative method is to keep θ fixed at a given angle and changing the wavelength of the x-ray source. This is usually done using a polyenergetic X-ray source where various wavelengths exist together, via the use of an X-ray tube. This is known as the energy dispersive method.

The phenomenon of low angle X-ray scattering LAXS or energy dispersive X-ray diffraction EDXRD can be exploited to characterize materials of low Z material. This is done by obtaining a diffraction pattern which, is a "signature" pattern specific of the material under investigation since it depends on the molecular structure. The diffraction pattern obtained is composed of the energy spectrum of incident X-ray source with diffraction effects superimposed upon it.

The LAXS/EDXRD technique has some solid theoretical and experimental support to be exploited in the field of material identification. It is not surprising to see that the first application of low angle X-ray scattering was a medical application, and in the field of radiology in particular, since all the previously mentioned works were in the field of radiology too. Harding *et al.* [10-11] experimented on a computed tomography imaging system based on low angle X-ray scattering.

The applications of low angle X-ray scattering are categorized mainly into two fields, the medical and industrial fields. The medical field will include computed tomography, bone mineral density determination [12], characterization of biomedical materials [13] and imaging. The industrial field will include studies of food

contaminants [14], spices [15], explosives [16-17] and other materials of interest [18].

EXPERIMENTAL PARAMETERS

The most important experimental parameters, which are used in setting up a photon scattering system, are photon sources, scattering material, detection method, shielding and collimation.

X-ray source

X-ray tubes are devices that produce a continuous energy spectrum with highly intense characteristic lines K_α, K_β, etc., that depends on the tube anode material. It is common in scattering experiments that the K-lines are used while all others including the bremstrahlung are removed, but in practice it is not feasible to eliminate completely the *bremstrahlung* part. However, in LAXS the total unfiltered spectrum will be used. Energy of such spectra depends on the voltage applied to the tube, and generally reaches up to 130 keV.

Scattering material

Ideally, a selected scattering material has to produce as large as possible scattering events when photons strike their scattering volumes. The scattering material also has to be of smaller dimensions to reduce both multiple scattering and angular spread. Area of target material is decided by the desired angular spread. Multiple scattering is reduced by the use of thin scatterers which is governed by the relation that the thickness of the material, $t << \frac{1}{\mu}$ where μ is the material's attenuation coefficient. However, sometimes, large size scattering materials need to be tested and in this case corrections have to be taken into account.

Materials differ in their structure into mainly three types; crystalline, amorphous and semi-amorphous. Crystalline materials are solid ones and possess very long-range order. Amorphous materials on the other hand do not have any order such as liquids and glasses. Semi-amorphous materials are the ones that possess some local order though not crystalline.

Method of detection

The job of any detector is to detect photons, but by virtue of its better resolution it can also differentiate between various photons of different energies such as elastic and inelastic scattered photons. Also, a detector with high efficiency can detect most of the photons incident to it. Unfortunately, resolution and efficiency are two competing parameters, high resolution requires the increase of purity of detecting material, fast collection time and lower noise, where as high efficiency is obtained by the increase of detector volume which implies increase in collection times, incomplete collection and recombination. The last factors lead to reduction in resolution of the detector. In addition to that it is very difficult to manufacture a high purity detecting material with such large volume requirements.

There are many types of detectors each with its own characteristics, employed in the field of photon detection. They can be divided into gas, scintillation and semiconductor detectors. Semiconductor detectors of type HPGe or Si (Li) are the most widely used with high resolution but with bulky liquid nitrogen dewars needed for operation.

Shielding and collimation

The need to maximize the intensity of the scattered radiation at the position of the detector, while at the same time reducing its angular spread and blocking all other unwanted radiation, is a fundamental requirement that experimentalists strive to achieve. The undesired radiation can be from the direct incident radiation, the scattered radiation from scattering equipments or from the surroundings, and can be from the common background radiation. Shielding of the detector is therefore necessary and this is accomplished usually by the use of blocks of lead with sufficient thickness. It is also recommended to place all equipments as far away from the walls and to locate equipments in the middle of the room to minimize scattered radiation reaching the detector, and to put all other photon emitting devices or materials at some safe place away from the detector. Collimation is of great importance in scattering experiments since it will increase the signal to noise ratio and hence increase the counting statistics of observing events. Also, a well-collimated beam gives a better definition of

scattering angle, and collimation defines the angular resolution and the scattering volume and its location within the target material. There exist two general types of collimators; pin-hole and slit collimators, but it should be understood that scattering from such collimators will occur and are named parasitic and edge scattering and they should be minimized.

EXPERIMENTAL SET UP AND RESULTS

The LAXS system under construction at the School of Physics, USM, has essentially the same parameters mentioned previously. The experimental set up is shown in Fig. (1).

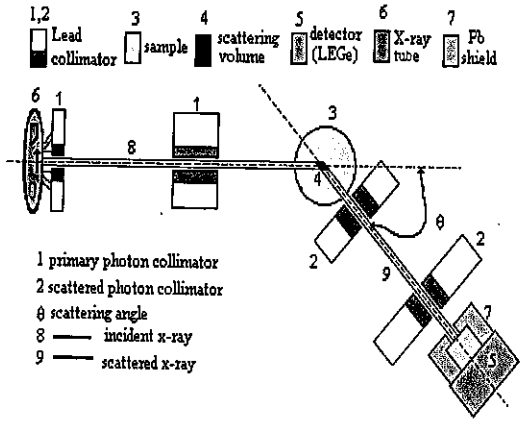

Fig.(1) Schematic diagram of LAXS system

X-ray tube and beam profile

The X-ray tube is a Philips PW 2273/20, high intensity tube with Cu or W anode and four Be windows each with thickness 300 μm. It has a long fine focus (LFF) and a focal spot of 0.4×12 mm^2. It can be operated at maximum voltage of 60 kV and maximum power rating of 2.2 kW. It is connected to a generator (Philips PW1830) which provides power to the tube, selection of voltage and current, shutter selection, and programmable and manual timing.

Experiments were conducted to test the shape, angular spread, angular deviation and intensity profile of the beam using the set up shown in Fig. (2). The images of X-ray beam, which were taken at various distances from tube aperture, were almost circular in shape and their diameters increase linearly with distance from the tube as shown on Fig. (3). The angular spread, 2β was found to be about 9°, where β is defined as the angle made by the beam from the top of the first image to the top of the remaining images. The angular deviation, α, which measures the depression of the X-ray beam from its straight-line position, was estimated to be in the range 4° - 5°.

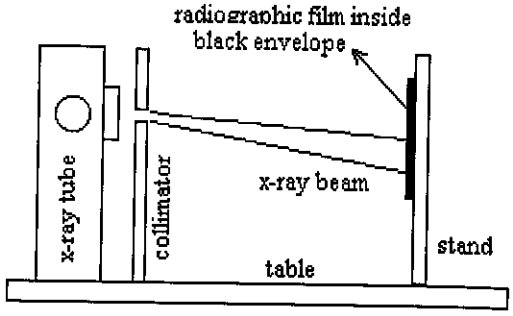

Fig. (2) Schematic diagram of the appratus

Beam intensity profile at various positions from the tube, was estimated by measuring the optical density (OD) of the images at such positions using a densitometer (RMI model 211C). An example of a graph of OD vs. distance across the image at distance 20 cm from the tube is given in Fig. (4). The OD is constant across the image and falls off at the edges for the curve of most of the positions from the tube taken in this experiment. The flat portion of the curves is therefore, representative of the image diameter. Some of the images obtained were smeared due to scattering caused by the source aperture. The flat region represents the actual diameter of the beam, which is consistent with the measured one.

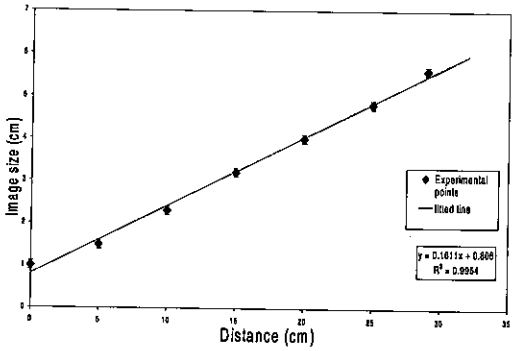

Fig. (3) Image Size (diameter) vs. Image distance from source collimator

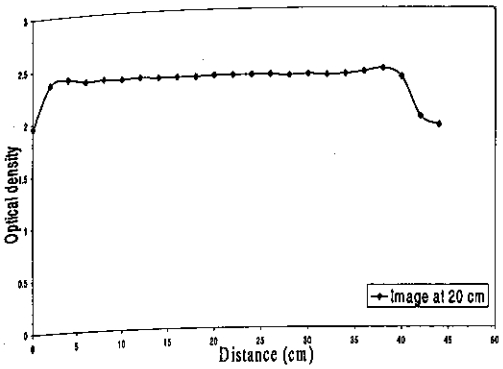

Fig.(4) Optical density vs. distance across image

Detector system

The detector employed in our system is a newly purchased Canberra LEGe planar detector, which is fabricated from germanium with a thin contact on the front face. The rear contact, which is the diffused contact, is less than the full passivated area. Thus capacitance of the detector is less than a planar device of similar size. The detector has an active area of 100 mm^2 and thickness 10 mm with a Be window of thickness 0.08 mm. The detector is operated at liquid nitrogen temperature. The signal from the detector is amplified and then analyzed using a Maestro II EG&G ORTEC PC based MCA system, which is used to process the signal. The detector was calibrated in the energy range 0 - 140 keV and was found to provide good linearity. Optimization of shaping times gave $\tau = 6$ μs. The resolution of the detector, represented by FWHM was measured for various energies as in Fig. (5). FWHM = 474 eV at 122 keV. The ratio FWTM/ FWHM, which is a good measure of closeness of the measured peaks to a Gaussian peak when it is less than 1.9, was found to fluctuate close to this value.

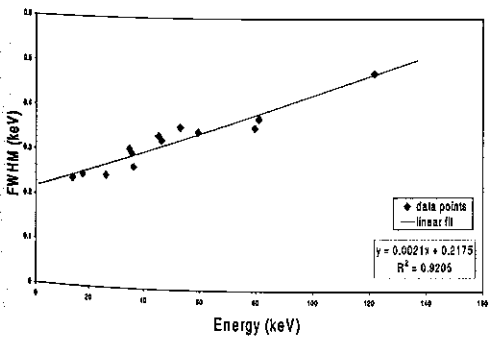

Fig. (5) FWHM vs. Energy for Ge det. (τ=6 μs)

Shielding, collimation, alignment and orientation

The detector head is shielded using lead blocks, and lead screen surrounds the apparatus to protect against scattered X-ray. Lead collimators, with slit and pin hole apertures of various sizes were made to fit in a stainless steel stand that moves on a track to adjust for distances and height. Alignment of the X-ray beam incident and scattered with the collimators and the detector is a precise operation that must be carried out carefully by monitoring the beam at all these positions. The distances between all the elements can be varied according to the requirements. Orientation of the system was achieved by fixing the scattering collimators and the detector on a movable arm that is pivoted at the sample to give the desired scattering angle. Low to high scattering angles can be selected.

DISCUSSION AND FURTHER WORK

The LAXS system has to go through some stages prior to reaching its objectives. The first is the geometrical optimization of the system and second the optimization of diffraction patterns and finally the development of the database materials.

The geometrical optimization is concerned with testing of all the possible factors that might have an effect on the diffraction pattern using samples of crystalline nature such as $CaCo_3$ or K_2HPO_4. The factors of influence are; scattering angles, distances, collimation shapes and sizes, tube voltages and currents, absorption, and multiple and incoherent scattering. Optimization of diffraction pattern will involve obtaining a well-resolved signature in a short time that will characterize the material.

No limit on the type of material that can be used by this method as long it has some order even on the local scale, and with low Z to avoid the high absorption cross-section.

Further studies can include the possible use of room temperature detectors to emphasize the element of robustness of the system and wide-angle scattering.

Acknowledgments Mr. N. A. Hussein would like to thank University of Garyounis for their scholarship. Technical assistance from Mr. Azmi Omar is greatly appreciated.

REFERENCES

1. Guinier, A. and Fournet, G. (1955). *Small angle scattering of X-rays*. New York: Wiley.
2. Magalhaes, S.D., Eichler, J., Goncalves, O.D., and Rizzo, P. (1995). *App. Rad. Isot.* **46**(6/7): 647-648.
3. Moore, R., Korbuly, D., and Amplatz, K. (1976). *Radiology* **120**: 713-717.
4. Joseph, P.M. and Spital, R.D. (1981). *Med. Phys.* **8**: 551.
5. Holt, R.S., Kouris, K., Cooper, M.J. and Jakson, D.F. (1983). *Phys. Med. Bio.* **28**(12): 1435-1440.
6. Holt, R.S., Cooper, M. J. and Jackson, D.F. (1984). *Nuc. Ins. Meth. Phys. Res.* **221**: 98-104.
7. Chong, C.S. (1989). *Proceedings of Regional Conference on Radiation Physics and Medical Physics*: 195-200.
8. Neitzel, U., Kosanetky, J. and Harding, G. (1985). *Phys. Med. Bio.* **30**(2): 1289-1296.
9. Johns, P.C. and Yaffe, M.J. (1983). *Med. Phys.* **10**(1): 40-50.
10. Harding, G., Kosanetzky, J. and Neitzel, U. (1985). *Phys. Med. Bio.* **30**(2):183-186.
11. Harding, G., Kosanetzky, J. and Neitzel, U. (1987). *Med. Phys.* **14**(4): 515-525.
12. Allday, A.W. and Farquharson, M.J. (2001). *Rad. Phys. Chem.* **61**: 589-592.
13. Kidane, G., Speller, R.D., Royle, G.J. and Hanby, A.M. (1999). *Phys. Med. Bio.* **44**: 1791-1802.
14. Bull, C.R., Zwiggelaar, R. and Speller, R.D. (1997). *Journal of Food Engineering* **33**: 167-179.
15. Desouky, O.S., Ashour, A.H., Abdullah, M.I. and Elshemey, W.H. (2002). *Rad. Phys. Chem.* **64**: 267-271
16. Luggar, R.D., Horrocks, J.A., Speller, R.D. and Lacey, R.J. (1997). *App. Rad. Isot.* **48**(2): 215-224.
17. Malden, C.H. and Speller, R.D. (2000). *Nuc. Instr. Meth. Phys. Res. A.* **449**: 408-415.
18. Bomsdorf, T.M. and Kosanetzky, J. (2000). *15th World Conference on NDT, Rome.*